KeA1

CHINESE ROOTS
GLOBAL IMPACT

Contents lists available at ScienceDirect

Petroleum Science

journal homepage: www.keaipublishing.com/en/journals/petroleum-science



Original Paper

Multichannel seismic resolution enhancement via spectral fitting for thin reservoir characterization



Si-Yuan Wang a, b, c, d, Hui Chen a, b, c, d, *, Ying Hu a, b, c, d, **, Xu-Ping Chen a, b, c, d

- ^a Key Laboratory of Earth Exploration and Information Techniques of Ministry of Education, Chengdu University of Technology, Chengdu, 610059, Sichuan,
- b State Key Laboratory of Geohazard Prevention and Geoenvironment Protection, Chengdu University of Technology, Chengdu, 610059, Sichuan, China
- ^c Geomathematics Key Laboratory of Sichuan Province, Chengdu University of Technology, Chengdu, 610059, Sichuan, China
- ^d School of Mathematical Sciences, Chengdu University of Technology, Chengdu, 610059, Sichuan, China

ARTICLE INFO

Article history: Received 29 May 2024 Received in revised form 25 November 2024 Accepted 7 April 2025 Available online 11 April 2025

Edited by Meng-Jiao Zhou

Keywords: Seismic processing High-resolution Spectral fitting Multichannel processing

ABSTRACT

As seismic signals propagate underground, the subsurface media absorb high—frequency components, decreasing seismic resolution and limiting the identification and characterization of thin reservoirs. To address the limitation, this paper proposes a multichannel spectral fitting (MSF) method. The MSF method aims to enhance seismic resolution by considering the spectral characteristics and the correlations between adjacent seismic traces. The key to the MSF method involves utilizing the amplitude spectrum of the attenuated Ricker wavelet to construct an objective function for spectral fitting, leading to improved seismic resolution. Furthermore, the MSF method establishes the correlation between adjacent seismic traces as a constraint to stably solve the target parameters based on the entire seismic spectrum, which helps obtain horizontally consistent and more realistic seismic signals. Synthetic and field seismic examples demonstrate that the proposed method not only provides higher-resolution seismic signals but also reveals more fine details of thin reservoirs compared to the time-variant spectral whitening method. It is concluded that the MSF method is a promising tool for seismic signal processing.

© 2025 The Authors. Publishing services by Elsevier B.V. on behalf of KeAi Communications Co. Ltd. This is an open access article under the CC BY license (http://creativecommons.org/licenses/by/4.0/).

1. Introduction

Thin reservoirs are widely developed in oil and gas basins within China and are essential targets for exploring lithological reservoirs. However, identifying thin reservoirs poses challenges due to the limited resolution of seismic signals (Alaei et al., 2018; Ni et al., 2022). To overcome this technical bottleneck, seismic interpreters detect subtle changes in the strata by analyzing the spectral response of seismic signals. For example, changes in amplitude (Widess, 1973) and peak frequency (Zhang and Castagna, 2011; Chen et al., 2023) of the spectrum can qualitatively or quantitatively identify the thickness of thin reservoirs based on tuning theory. On the other hand, various methods have been proposed to broaden the frequency bandwidth, which can improve

E-mail addresses: huichencdut@cdut.edu.cn (H. Chen), huying15@cdut.edu.cn (Y. Hu).

the vertical resolution of seismic signals, including Q compensation (Liu et al., 2023; Mu et al., 2023; Xu et al., 2023; Wu et al., 2024), deconvolution (Margrave and Lamoureux, 2001; Lan et al., 2023), spectral whitening (Lee, 1986), and others (Sajid and Ghosh, 2014; Zhang et al., 2023; Yang et al., 2024). These methods have been successfully applied in production, but each has distinct applicability and limitations. Spectral whitening and its variations (Naghadeh and Morley, 2017) aim to enhance seismic resolution by capturing all frequencies within the seismic signal's useful band. This method is simple in principle and computationally efficient, making it widely used in practical processing, but an incorrect window length may lead to unsatisfactory results (Hu et al., 2020). Unlike spectral whitening methods, deconvolution methods such as homomorphic deconvolution (Jin and Eisner, 1984) and predictive deconvolution (Gibson and Larner, 1984) estimate and compress seismic wavelets to improve the resolution of seismic signals. However, wavelet compression may increase high-frequency noise. directly impacting reservoir prediction accuracy (Guo et al., 2022).

Rosa and Ulrych (1991) introduced the spectral fitting deconvolution method. This method assumes a smooth wavelet spectrum

^{*} Corresponding author.

^{**} Corresponding author.

and employs polynomial fitting to match the spectrum of seismic signals with that of the seismic wavelet, thereby broadening the wavelet amplitude spectrum and enhancing the resolution. Over recent decades, rapid developments have occurred in spectral fitting techniques. For example, Li et al. (2013) proposed an adaptive spectral fitting deconvolution method using the signal-to-noise ratio as a constraint. Chen et al. (2014) used the frequency scaling factor to stretch the seismic wavelet's frequency band after extracting its amplitude spectrum. In addition to implementing deconvolution in the frequency domain, Margrave et al. (2002, 2005) extended the method to the time-frequency domain using the Gabor transform and proposed time-frequency domain deconvolution, which greatly improved the deconvolution effect. However, the time window of the Gabor transform is fixed, which makes it inflexible in practical applications (Zhou et al., 2014). With the development of time-frequency analysis, the S transform was proposed (Stockwell et al., 1996), which is more flexible than the Gabor transform. Based on the advantages of the S transform, Zhou et al. (2014) introduced Gabor deconvolution into the S transform domain, improving the accuracy of deconvolution. Wang et al. (2017) used the secondary time-frequency spectrum of the S transform to construct a two-dimensional filter that adaptively determines the frequency expansion range. Wu and Castagna (2017) found that the spectrum of the S transform shifts upward and proposed the unscaled S transform (UST) to prevent the frequency shift in the spectrum. Based on the idea of spectral fitting, some other high-resolution processing methods have been proposed. For example, Tang et al. (2010) performed two Fourier transform analyses on seismic signals and developed a quadratic spectrum method to improve seismic resolution. Deng et al. (2023) constrained the target wavelet with the seismic spectrum, expanding the seismic frequency bandwidth and improving the resolution of seismic signals effectively.

In fact, as seismic wavelets propagate underground, factors like geometrical spreading, absorption, and scattering decrease the amplitude. Absorption particularly affects seismic resolution (Dasgupta and Clark, 1998). Therefore, the wavelet spectrum used for spectral fitting should also consider this absorption attenuation. Furthermore, most of these methods process seismic traces individually and then perform joint analysis without considering the interrelations between adjacent traces. However, seismic signals are recorded in the form of multichannel. Single trace processing lacks lateral information, which may lead to discontinuities in geological information that confuse the interpreters (Wu et al., 2020). Recently, multichannel deconvolution methods that consider certain prior constraints in the objective function have been gradually developed, improving the lateral continuity of the inversion results (Ma et al., 2017; Zhang et al., 2022). Thus, we can employ multichannel processing to ensure the lateral continuity of high-resolution seismic signals.

This paper introduces a multichannel spectral fitting (MSF) method to identify thin reservoirs. The first step involves constructing the target equation using the spectrum of the attenuated Ricker wavelet to enhance the vertical seismic resolution. Next, multichannel constraints are employed to solve the target parameters stably and thus maintain the continuity of seismic signals. This paper is organized as follows. Section 2 provides the theoretical formulas of the proposed MSF method. In Sections 3 and 4, we demonstrate the feasibility and effectiveness of the MSF method in thin reservoir identification using synthetic and field seismic examples. Finally, Section 5 presents the conclusions.

2. Method

Step 1: According to the nonstationary convolution model (Sheriff and Geldart, 1995; Margrave, 1998), the seismic signal can be expressed as

$$s(t) = w(t,\tau) * r(t) = \int_{-\infty}^{+\infty} w(t-\tau,\tau)r(\tau)d\tau$$
 (1)

where * and τ denote the convolution operation and time variable, respectively. Symbols $w(t,\tau)$ and r(t) mean the dynamic wavelet and reflectivity.

Seismic signals attenuate during underground propagation. The seismic attenuation includes geometric expansion, scattering, and absorption attenuation, among which absorption attenuation has a wide impact on seismic resolution (Dasgupta and Clark, 1998). The attenuation function a(t,f) is used to describe the absorption attenuation:

$$|a(t,f)| = e^{-\alpha tf} \tag{2}$$

where α is the attenuation factor. By combining Eq. (1) and Eq. (2), the frequency domain attenuation convolution model is obtained as follows:

$$\widehat{\mathbf{s}}(f) = \widehat{\mathbf{w}}(f) \int_{-\infty}^{+\infty} a(t, f) r(t) e^{-2\pi i f t} dt$$
(3)

where $\widehat{s}(f)$ and $\widehat{w}(f)$ are calculated by the Fourier transform, which represent the frequency spectrum of the attenuated seismic signal and the frequency spectrum of the source seismic wavelet. Thus, we have

$$s(t) = \int_{-\infty}^{+\infty} \int_{-\infty}^{+\infty} \widehat{w}(f)a(u,f)r(u)e^{2\pi i f(t-u)}dfdu$$
 (4)

where *u* denotes the time variable.

Step 2: The UST of s(t) is defined as (Wu and Castagna, 2017)

$$V_g s(\tau, f) = \int_{-\infty}^{+\infty} s(t)g(\tau - t, f)e^{-2\pi i f t} dt$$
 (5)

where $g(\tau - t, f) = \frac{1}{\sqrt{2\pi}} e^{-\frac{(\tau - t)^2 f^2}{2}}$ is the window. Substituting Eq. (4) into Eq. (5) gives

$$V_{g}s(\tau,f) = \int_{-\infty}^{+\infty} \left(\int_{-\infty}^{+\infty} \int_{-\infty}^{+\infty} \widehat{w}(\xi) a(u,\xi) r(u) e^{2\pi i \xi(t-u)} d\xi du \right)$$

$$g(\tau - t,f) e^{-2\pi i f t} dt$$
(6)

where ξ denotes the frequency variable.

Then the asymptotic result for Eq. (6) can be derived as (Margrave et al., 2002; Zhou et al., 2024)

$$|V_g s(\tau, f)| \approx |\widehat{w}(f)| |a(\tau, f)| |V_g r(\tau, f)|$$
(7)

where $|\cdot|$ denotes absolute values. We now assume that the UST of the reflectivity, $|V_g r(\tau,f)|$, is white with a mean of unity, which means that the spectral shape of seismic wavelets $|\widehat{w}(f)| |\alpha(\tau,f)|$ primarily provides the general shape, while $|V_g r(\tau,f)|$ provides only

the detail of $|V_g s(\tau, f)|$ (Grossman et al., 2001; Margrave and Lamoureux, 2001). Thus, we rewrite Eq. (7) as

$$S(\tau, f) = \widehat{W}(f)e^{-\alpha\tau f} \tag{8}$$

where $S(\tau, f) = |V_g s(\tau, f)|$, $\widehat{W}(f) = |\widehat{w}(f)|$.

Step 3: The Ricker wavelet finds extensive application in seismic signal processing and interpretation, including seismic to well tie, quality-factor estimation, and forward modeling (Gholamy and Kreinovich, 2014; Mamasani et al., 2017). The frequency domain representation of the Ricker wavelet is

$$W(f, f_{\rm d}) = \frac{2}{\sqrt{\pi}} \frac{f^2}{f_{\rm d}^3} e^{\frac{-f^2}{f_{\rm d}^2}}$$
 (9)

where f_d is the dominant frequency of the wavelet. Its mean f_m and variance f_σ can be expressed as (Zhang et al., 2017)

$$f_{\rm m} = \frac{\int_0^{+\infty} fW(f, f_{\rm d}) df}{\int_0^{+\infty} W(f, f_{\rm d}) df} \approx 1.06 f_{\rm d}$$
 (10)

$$f_{\sigma} = \sqrt{\frac{\int_{0}^{+\infty} (f - f_{\rm m})^2 W(f, f_{\rm d}) df}{\int_{0}^{+\infty} W(f, f_{\rm d}) df}} \approx 0.34 f_{\rm d}$$
(11)

In many seismic explorations, the source wavelet spectrum with no attenuation can be approximated by the Ricker spectrum (Ricker, 1953; Zhang and Ulrych, 2002), that is

$$\widehat{W}(f) \approx AW(f, f_{\rm d}) \tag{12}$$

where A means the amplitude coefficient of the Ricker wavelet. Combining Eq. (8) and Eq. (12), we have

$$S(\tau, f) \approx AW(f, f_d)e^{-\alpha \tau f}$$
 (13)

where has parameters α . To obtain α , we can establish an objective function, based on Eq. (13):

$$\underset{A_{\tau},f_{d},\alpha_{\tau}}{\operatorname{argmin}} \left\{ \sum_{n}^{N} \left\| S(\tau,f_{n}) - A_{\tau}W(f_{n},f_{d}) e^{-\alpha_{\tau}\tau f_{n}} \right\|_{2}^{2} \right\}$$
(14)

where $\|\cdot\|_2$ represents L₂-norm. The symbol N is the number of frequency points for fitting. The symbol f_n means the n-th frequency point. A_{τ} and α_{τ} mean the amplitude coefficient and the attenuation factor at time τ . By solving this function, we can obtain the attenuation factor.

Step 4: Eq. (14) solves the objective function of the seismic traces individually and then forms a solution vector. However, the solution for a single trace is easily affected by noise or complex structures, resulting in abnormal values and reducing the spatial continuity of seismic signals (Gao et al., 2014; Guo et al., 2022). While underground strata are not uniform in the lateral direction, the lateral variation of the sedimentary strata is relatively stable, showing local lateral continuity and similarity in adjacent seismic traces (Dai and Yang, 2022). Therefore, it can be considered that the attenuation in adjacent seismic traces at the same time is locally similar. This similarity can be used to

formulate joint vertical and horizontal constraints on the target parameters, thereby enhancing the stability of the target parameter solution.

We introduce a penalty term that contains time and seismic trace information into the objective function. Finally, we solve the following least squares problem to estimate $\alpha_{\tau,c}$:

$$\underset{A_{\tau,c},f_{d_{c}},\alpha_{\tau,c}}{\operatorname{argmin}} \left\{ \sum_{n}^{N} \left\| S(\tau,f_{n},c) - A_{\tau,c}W(f_{n},f_{d_{c}}) e^{-\alpha_{\tau,c}\tau f_{n}} \right\|_{2}^{2} + u_{1} \|A\|_{2}^{2} + u_{2} \|f_{d}\|_{2}^{2} + u_{3} \|\alpha\|_{2}^{2} \right\}$$

$$(15)$$

where c is the trace number. $A_{\tau,c}$ and $\alpha_{\tau,c}$ represent the amplitude coefficient and the attenuation factor at c-th trace and time τ , respectively. The symbol $f_{\rm d_c}$ means the dominant frequency of the Ricker wavelet at c-th trace. Symbols u_1 , u_2 , and u_3 are regularization parameters, which are employed to balance the respective constraints. Optimizing the regularization parameters is a complex issue, and we determine them through trials. The optimal attenuation factor can be obtained by solving Eq. (15) using the Matlab optimization toolbox.

Step 5: Once we obtain $\alpha_{\tau,c}$, The spectrum of the high-resolution seismic signal at c-th trace is

$$S_{h}(\tau, f, c) = S(\tau, f, c)e^{\alpha_{\tau, c}\tau f}$$
(16)

However, the spectrum obtained using Eq. (16) contains high-frequency noise. Due to the absorption attenuation of seismic signals during propagation, the spectrum of the source wavelet has the broadest frequency range. When broadening the bandwidth of seismic signals, it is necessary to filter out amplitude values above this frequency range to suppress high-frequency noise. For each seismic trace, consider the following filter:

$$F(f,c) = \begin{cases} 1, f \le f_{m_c} + 4f_{\sigma_c} \\ \frac{f_{m_c} + 6f_{\sigma_c} - f}{2f_{\sigma_c}}, f_{m_c} + 4f_{\sigma_c} < f \le f_{m_c} + 6f_{\sigma_c} \\ 0, f > f_{m_c} + 6f_{\sigma_c} \end{cases}$$
(17)

where f_{m_c} and f_{σ_c} represent the mean and standard deviation of the Ricker wavelet at c-th trace, and are related to f_{d_c} . Combining Eqs. (10), (11) and (17), we have

$$F(f,c) = \begin{cases} 1, & f \le 2.42f_{\rm d} \\ \frac{3.1f_{\rm d} - f}{0.68f_{\rm d}}, & 2.42f_{\rm d} < f \le 3.1f_{\rm d} \\ 0, & f > 3.1f_{\rm d} \end{cases}$$
(18)

where designed based on the sigma criterion and can retain most of the information within the frequency band of the source seismic wavelet. This ensures that no useful signals are filtered out. Combining Eq. (16) and Eq. (18), the time-frequency spectrum of the *c*-th high-resolution seismic signal can be determined by

$$S_{h}(\tau, f, c) = F(f, c)S(\tau, f, c)e^{\alpha_{\tau, c}\tau f}$$
(19)

Finally, we use the inverse UST to get the high-resolution signal:

$$S_{\rm h}(t,c) = \int_{-\infty}^{+\infty} \int_{-\infty}^{+\infty} S_{\rm h}(\tau,f,c) |f| e^{i2\pi f t} d\tau df \tag{20}$$

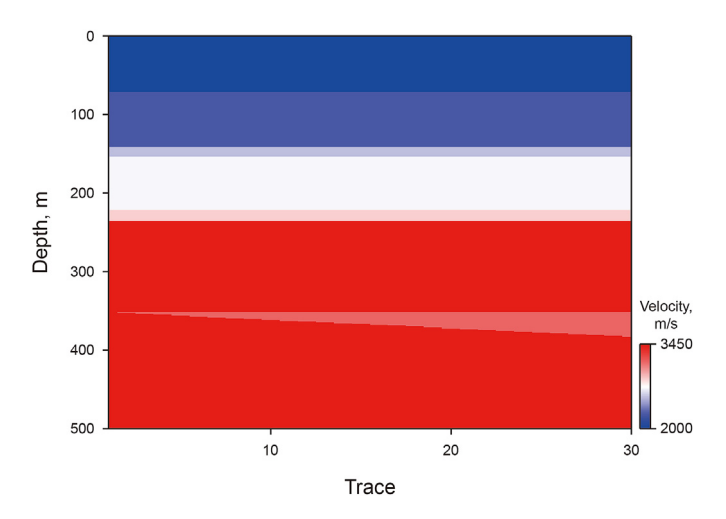


Fig. 1. Synthetic noise-free velocity model.

3. Synthetic examples

3.1. Synthetic noise-free example

In order to evaluate the effects of the MSF method on improving

seismic data resolution, we design a noise-free example. The model consists of a horizontal layer, two thin layers, and a wedge-shaped layer. The first layer, located at a depth of 140 m, has a thickness of 11 m, while the second layer, at a depth of 220 m, has a thickness of 13 m. The trace interval is 2 m, the sampling interval is 1 ms, and the velocity of the wedge is 3150 m/s.

In Fig. 2(a), the synthetic seismic response is obtained by convolving the 40 Hz Ricker wavelet with the reflectivity calculated in Fig. 1. Chung and Lavvton (1995) demonstrated that the tuning thickness of the thin layer illuminated by the Ricker wavelet is $T_{\rm R}=\frac{\sqrt{6}}{2\pi f_{\rm d}}$. For the above model, $T_{\rm R}=9.7$ ms, near trace 20. Fig. 2(b) shows the attenuated synthetic seismic signal with Q=50. We first observe two thin layers. Due to the low resolution, the thin layers in Fig. 2(a) and (b) cannot be identified. Fig. 2(c) and (d) display the results of the time-variant spectral whitening (TVSW) and MSF methods. Both methods effectively enhance seismic resolution and identify the two thin layers. Nevertheless, the MSF method better resolves the thin bed compared to the result obtained using the TVSW method.

Fig. 3(a)—(d) show the enlarged results of the red rectangle in Fig. 2(a)—(d) to better compare the wedge-shaped layer results. In Fig. 3(a), the unresolved event of the wedge is separated near trace 20. With the addition of attenuation, the seismic signal resolution

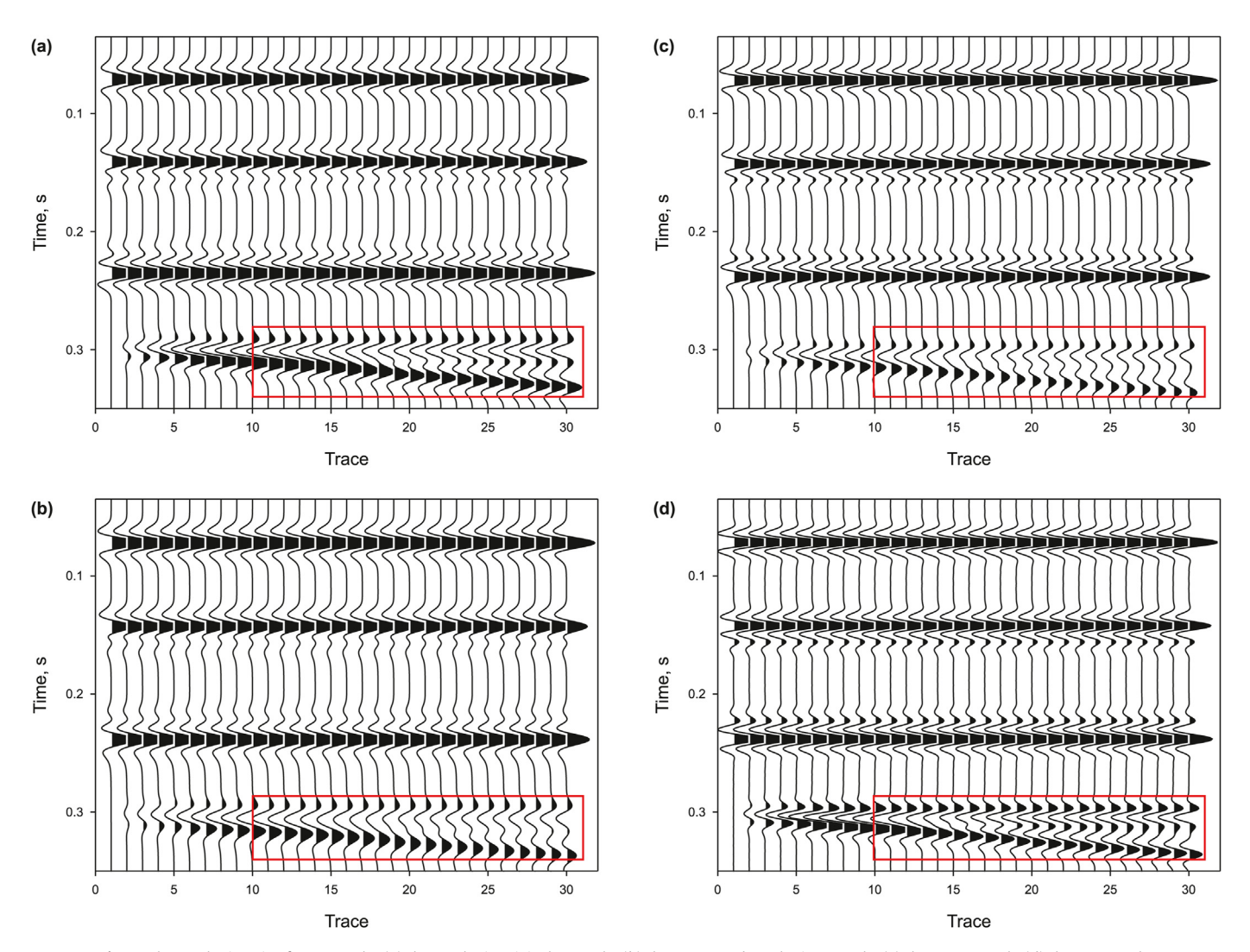


Fig. 2. The synthetic noise-free example: (a) the synthetic original example, (b) the attenuated synthetic example, (c) the TVSW result, (d) the MSF result.

decreases, and the resolved thickness of the wedge occurs near trace 26, corresponding to a layer thickness of 12.6 ms, as Fig. 3(b) shows. After TVSW, the wedge-shaped layer can be identified at trace 22, corresponding to a thickness of 10.6 ms, as shown in Fig. 3(c). The resolution limit of the proposed MSF for the wedge-shaped layer appears near trace 18, corresponding to 8.6 ms, which is better than the TVSW method, as shown in Fig. 3(d). Fig. 4(a) depicts the Fourier spectra of the above signal, represented

in purple, blue, yellow, and red lines, respectively. It is evident that the frequency bandwidth experiences a significant widening after employing the MSF method. Hence, the MSF method is more effective and satisfactory for improving seismic signal resolution and characterizing thin reservoirs.

In the experiment, we optimize the regularization parameters by calculating the average correlation coefficient between the reconstructed and original signals (Du et al., 2018). Testing reveals

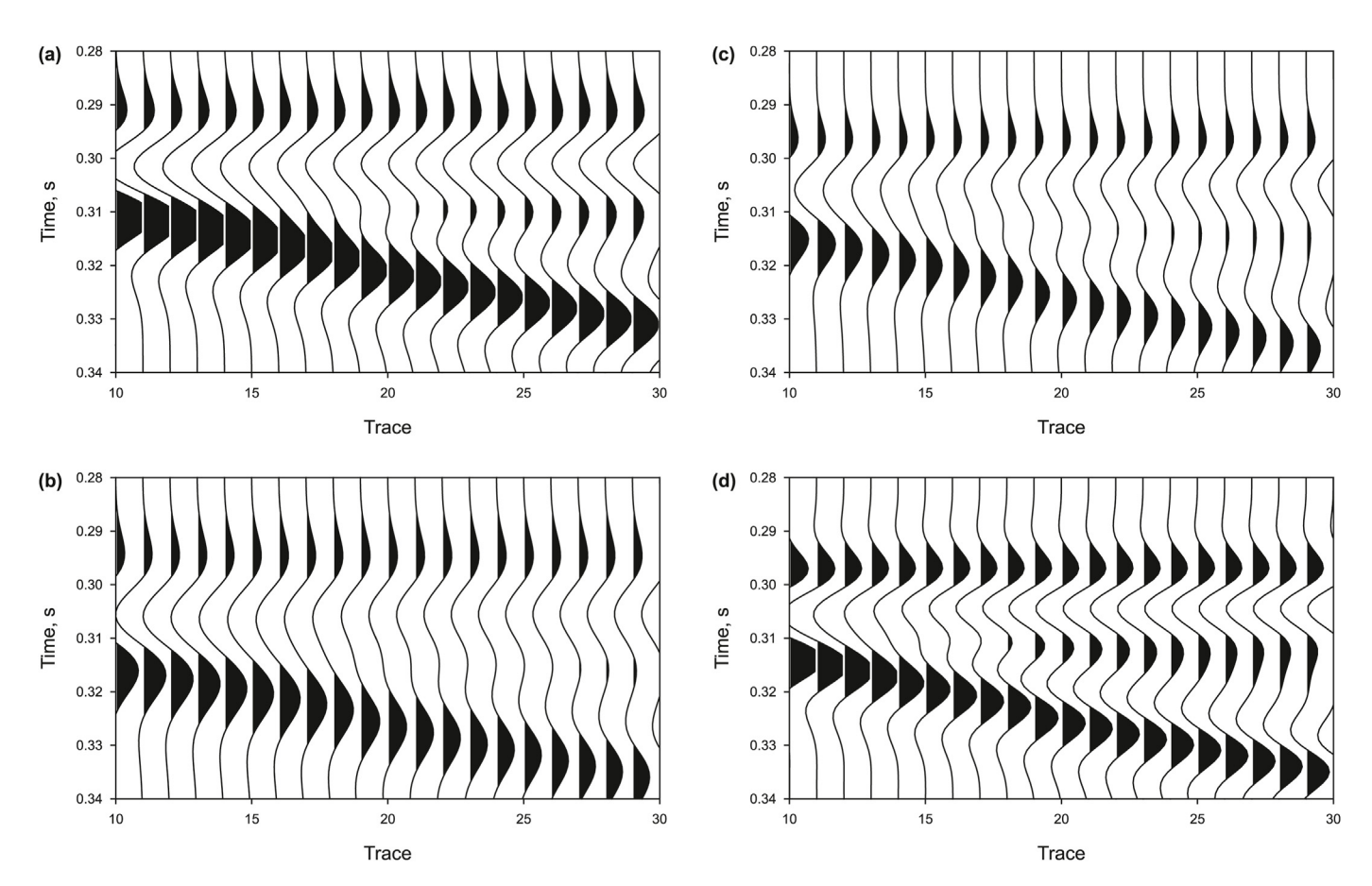


Fig. 3. The enlarged results in the red rectangle in Fig. 2: (a) the synthetic original example, (b) the attenuated synthetic example, (c) the TVSW result, (d) the MSF result.

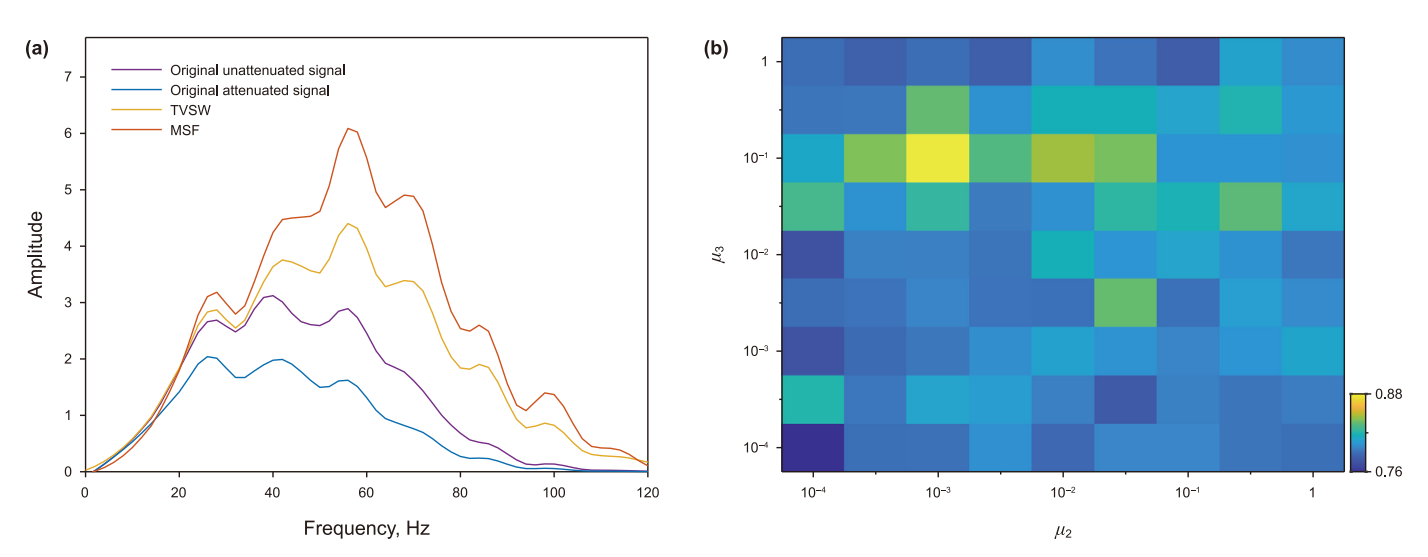


Fig. 4. (a) Fourier spectra comparison, (b) regularization parameter optimization based on correlation analysis.

that the values of u_2 , and u_3 are dominant, while changes in u_1 have minimal impact. The average correlation coefficient under different u_2 and u_3 values is calculated to determine the optimal regularization parameter. Fig. 4(b) shows the correlation coefficient values with changes in u_2 and u_3 , indicating that the highest correlation coefficient is obtained when $u_2 = 0.001$ and $u_3 = 0.1$, which are the optimal regularization parameters.

3.2. Synthetic noisy example

The second example is the Marmousi example, which is used to verify the robustness and stability of the MSF method in complex and noisy geological conditions. This paper convolves the velocity model (Wang et al., 2019) with the 30 Hz Ricker wavelet to obtain the Marmousi example in the time domain, which has a sampling interval of 8 ms, totaling 663 traces. Fig. 5(a) shows the obtained example with 10 dB random noise. On this basis, the Q model (Wang et al., 2019) is added to obtain Fig. 5(b). Fig. 5(c)—(f) show

the enlarged results of the yellow and blue rectangles in Fig. 5(a) and (b), respectively. Comparing Fig. 5(e) with Fig. 5(c), it can be seen that, due to the influence of noise and energy attenuation, the reflective interfaces in Fig. 5(e) are challenging to distinguish. Meanwhile, identifying and tracking seismic events becomes more difficult in Fig. 5(f) compared to Fig. 5(d).

Fig. 6(a) and (b) show the processing results of the TVSW and MSF methods. The enlarged results of the yellow and blue rectangles in Fig. 6(a) and (b) are shown in Fig. 6(c)—(f). Overall, both methods improve the resolution of the signals compared to Fig. 5(b). However, as observed in Fig. 6(c)—(f), there are differences between the results of the TVSW and MSF methods. While the TVSW method improves the imaging quality of seismic signals, it disrupts the continuity of seismic reflection, as shown in Fig. 6(c). As shown in Fig. 6(e), the thin reservoir details are well revealed. Additionally, the MSF preserves the lateral continuity of the section, benefiting from its multichannel constraints and filtering approach. A comparison of Fig. 6(d) with Fig. 6(f) demonstrates that the MSF

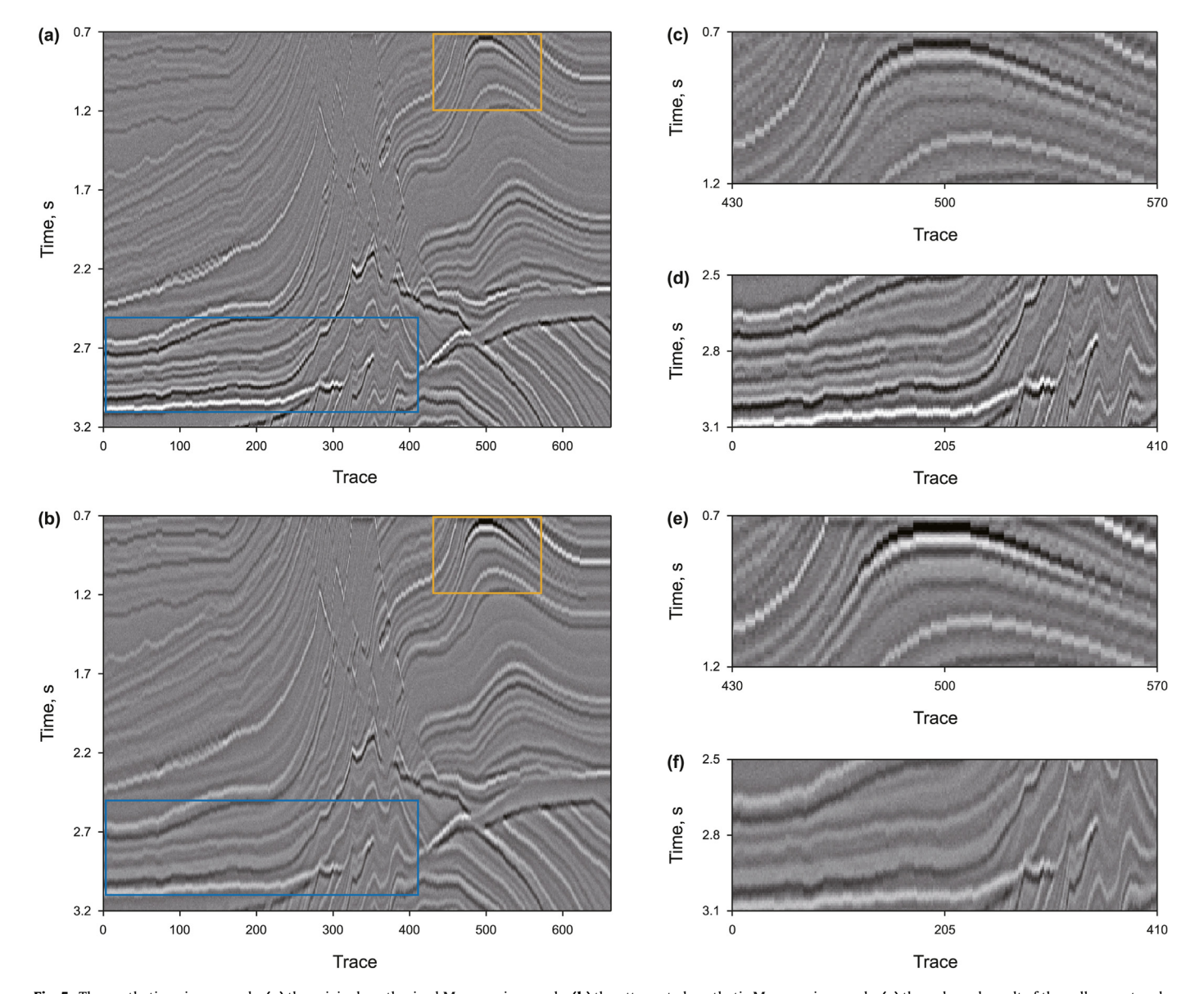


Fig. 5. The synthetic noisy example, (a) the original synthesized Marmousi example, (b) the attenuated synthetic Marmousi example, (c) the enlarged result of the yellow rectangle in (a), (d) the enlarged result of the blue rectangle in (b).

method significantly enhances the resolution of seismic signals and provides a clearer identification of seismic events compared to the TVSW method. These benefits demonstrate that the proposed MSF has advantages in identifying thin reservoirs.

4. Field data example

We apply the proposed MSF to gas-bearing tight sandstone reservoirs in the Sichuan Basin of China to validate its practicability. Seismic signals in this area have a narrow bandwidth due to energy attenuation, which affects the identification of geological targets. Fig. 7(a) is the original seismic section comprising 300 seismic traces, each sampled at 2 ms intervals. The green line represents well A. In low-quality seismic signals, the indistinct reflection layer makes it challenging to track certain seismic events. Therefore, enhancing the vertical resolution of seismic signals is essential for improving the geological body characteristics and well location deployment of existing data. Fig. 7(b) and (c) display the results after applying the TVSW and the proposed MSF. By comparing

Fig. 7(b) and (c) with Fig. 7(a), we observe that both methods improve the vertical resolution and show more detailed reflections. In Fig. 7(b), the red ellipses highlight that the TVSW method results in lateral discontinuities, possibly due to excessive high-frequency noise introduced during processing. In the MSF method, the stability of multichannel processing and the suppression of high-frequency noise contribute to better continuity of the seismic section, as shown in the red ellipses in Fig. 7(c). In addition, we extract three seismic signals near the seismic trace through the well, named trace 229, trace 230, and trace 231. The average amplitude spectra are shown in Fig. 7(d). The frequency band comparison reveals that the MSF method effectively compensates for energy in the high-frequency compared to the original seismic section and the TVSW result.

To compare the ability of different methods to identify thin reservoirs more clearly, we enlarge the results displayed in the black rectangular box of Fig. 7(a)—(c), as shown in Fig. 8. Furthermore, the gamma-ray (GR) of well logs is employed to verify the validity of the high-resolution results. The black arrow in

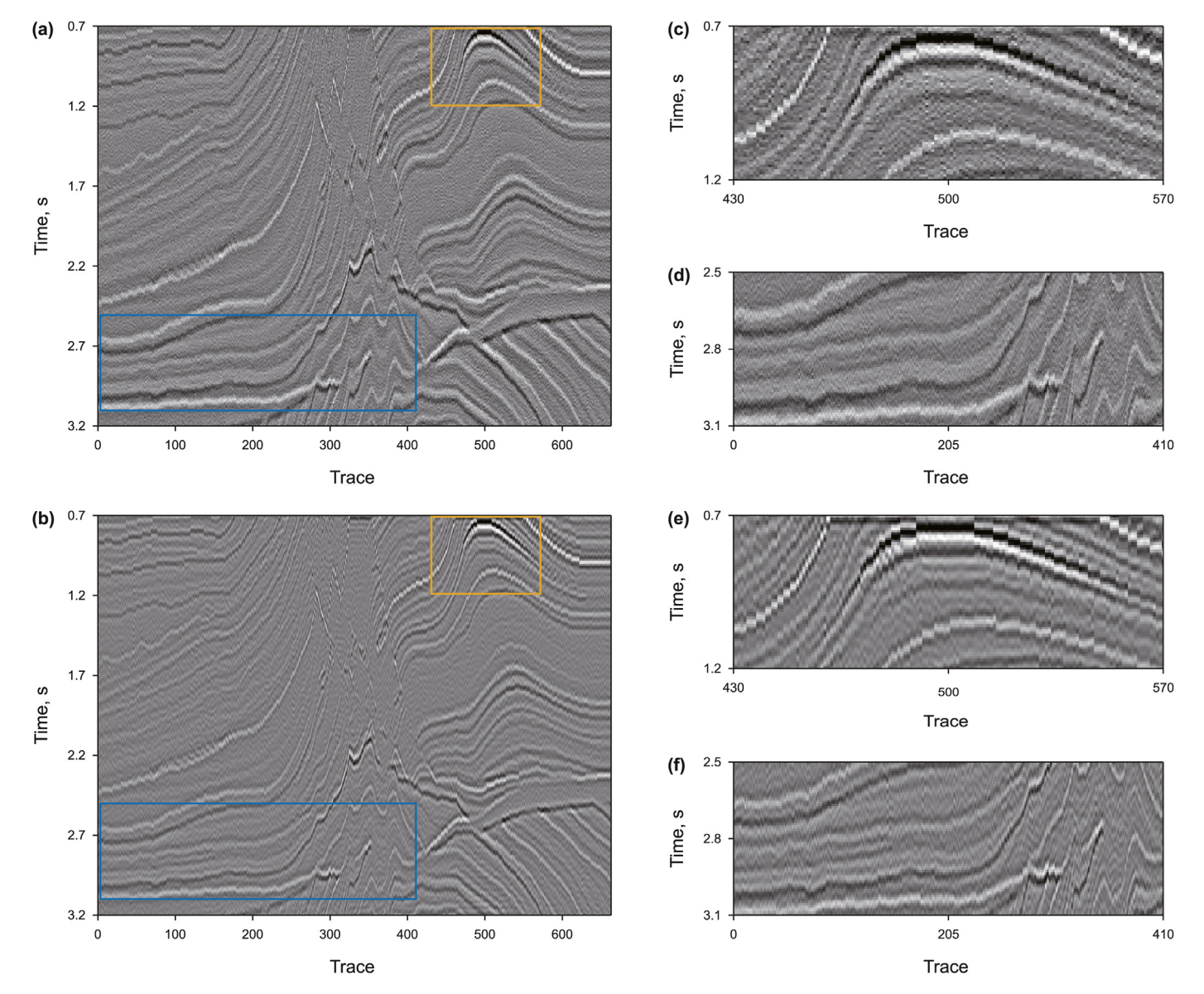


Fig. 6. The synthetic noisy example, (a) the TVSW result, (b) the MSF result, (c) the enlarged result of the yellow rectangle in (a), (d) the enlarged result of the blue rectangle in (a), (e) the enlarged result of the yellow rectangle in (b).

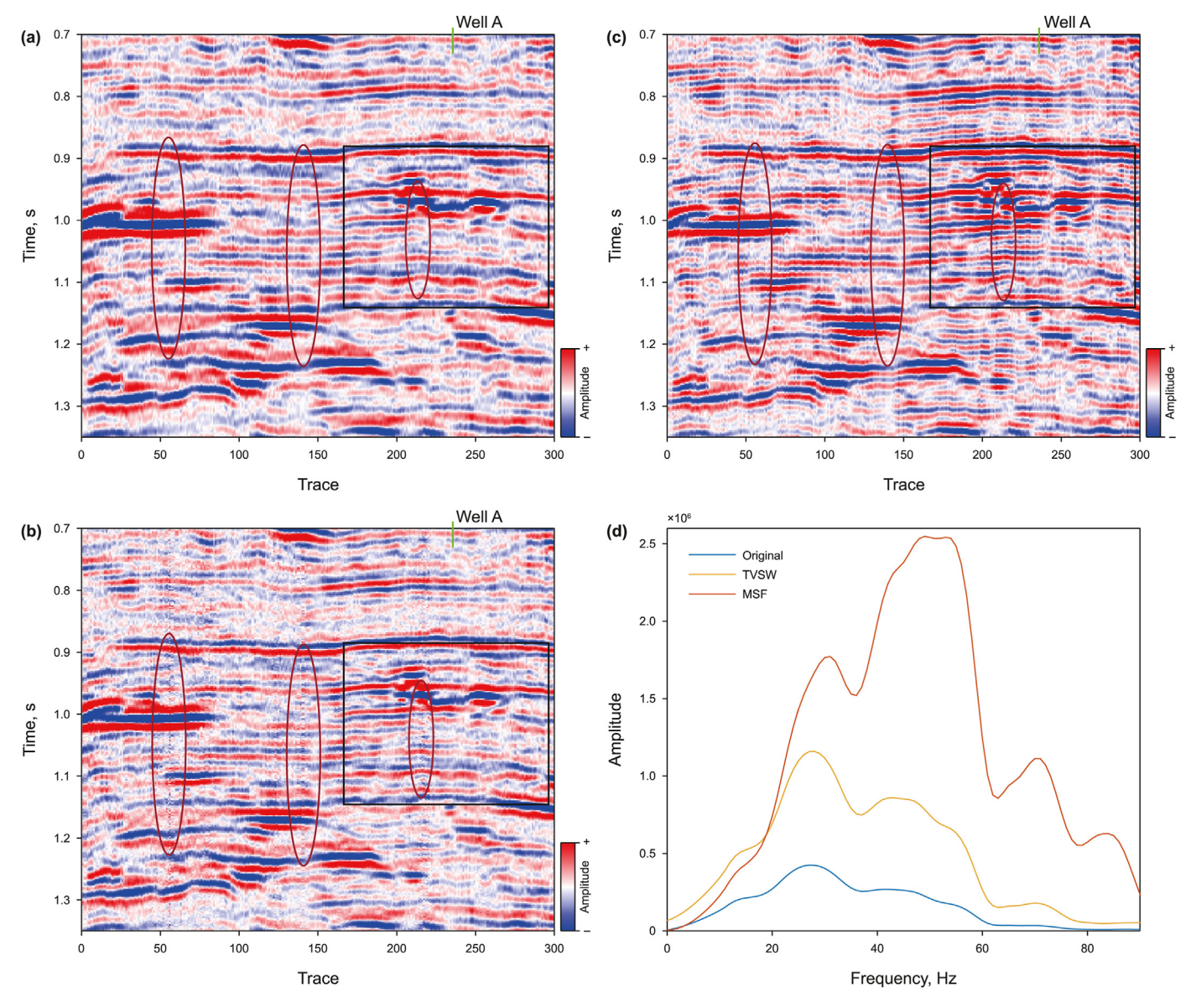


Fig. 7. Field seismic section, (a) the original section, (b) the TVSW result, (c) the MSF result, (d) amplitude spectra comparison.

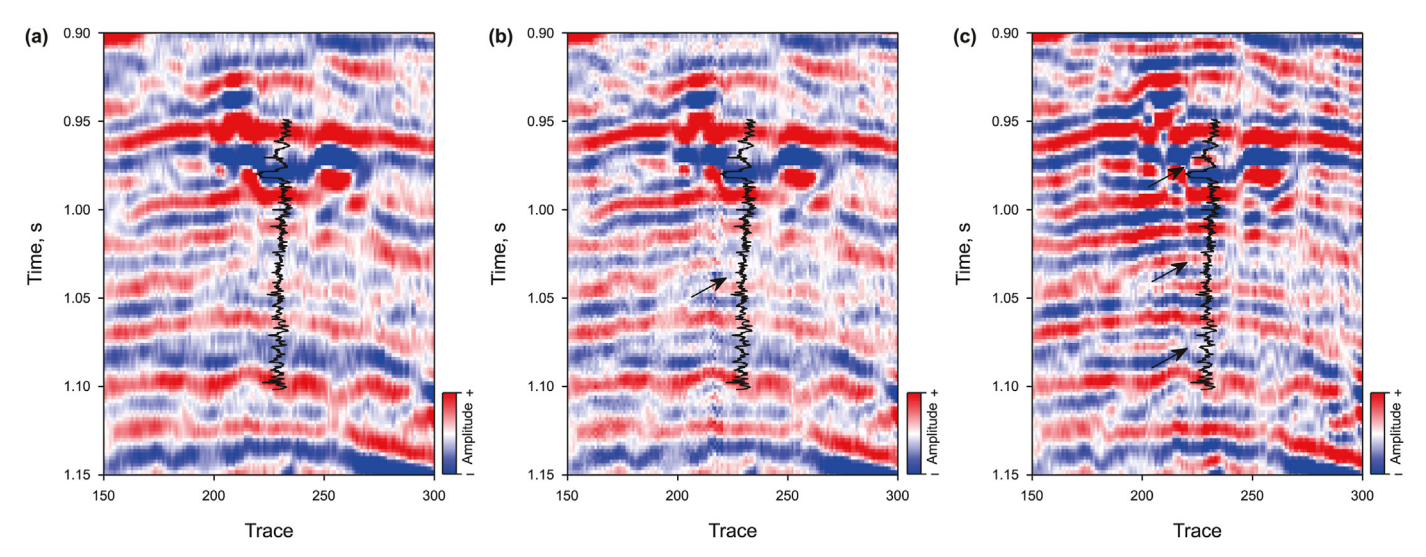


Fig. 8. The enlarged results of the black rectangle in Fig. 7, (a) the original section, (b) the TVSW result, (c) the MSF result.

Fig. 8(b) indicates a new seismic event detected by the TVSW method. This event is also identified using the proposed method. Moreover, the MSF method detected two additional seismic events, as shown in Fig. 8(c). These three seismic reflection events can be interpreted as sandstone reservoirs and confirmed by the GR log. Overall, both methods effectively improve the seismic resolution. The proposed MSF significantly enhances the resolution of seismic signals, revealing fine details of thin reservoirs.

5. Conclusions

This paper proposes a novel method called MSF to enhance seismic resolution, which is applied and analyzed in thin reservoir characterization. The effectiveness and accuracy of the MSF method are verified using synthetic and field seismic examples and are compared with the TVSW method. Based on the analysis above, the following conclusions can be drawn.

- The MSF method extends the bandwidth of seismic signals by fitting the spectrum of the attenuated Ricker wavelet, thus improving the seismic resolution.
- (2) The MSF method's multichannel constraint ensures the stability of the parameter solution and helps maintain the lateral continuity of seismic signals, making it more conducive to seismic interpretation.
- (3) The proposed MSF method maintains the lateral continuity of seismic signals while improving the seismic resolution, demonstrating its advantages in thin reservoir characterization.

CRediT authorship contribution statement

Si-Yuan Wang: Writing — original draft, Methodology. **Hui Chen:** Writing — review & editing, Funding acquisition. **Ying Hu:** Resources. **Xu-Ping Chen:** Investigation.

Declaration of competing interest

The authors declare that they have no known competing financial interests or personal relationships that could have appeared to influence the work reported in this paper.

Acknowledgments

The authors would like to thank the editors and reviewers for their constructive comments, which will greatly help improve the quality of this paper. This work was supported in part by the National Natural Science Foundation of China under Grant 42174164 and Grant 41704132; in part by the Key Program of the Joint Fund of the Science, Technology, and Education of Sichuan Province, China under Grant 2024NSFSC1955; in part by the Natural Science of Sichuan Province, China under 2024NSFSC0080; in part by the State Key Laboratory of Geohazard Prevention and Geoenvironment Protection Independent Research Project under Grant SKLGP2022Z011; in part by the Chengdu University of Technology Postgraduate Innovative Cultivation Program: Spatiotemporal Characterization of Seismic Signals for Tight Channel Sandstone Gas Reservoirs in the Synchro-Squeezing/ Extracting Transform Domain under Grant CDUT2023BJCX002; in part by the Creative Research Groups of the Natural Science Foundation of Sichuan under Grant 2023NSFSC1984; 14th Five Year Plan Major Science and Technology Project of CNOOC under Grant KJGG2022-0903.

References

- Alaei, N., Roshandel, K.A., Kamkar, R.A., et al., 2018. Seismic resolution enhancement using scale transform in the time-frequency domain. Geophysics 83 (6), V305–V314. https://doi.org/10.1190/geo2017-0248.1.
- Chen, S.Q., Li, X.Y., Di, B.R., et al., 2014. A novel method for enhancing resolution using scale transforms. 76th Eur. Assoc. Geosci. Eng. Conf. Exhib. 2014 Exp. Energy Inc. SPE Eur. 1, 1—5. https://doi.org/10.3997/2214-4609.20141595.
- Chen, X.P., Chen, H., Hu, Y., et al., 2023. Statistical synchrosqueezing transform and its application to seismic thin interbed analysis. IEEE Trans. Geosci. Rem. Sens. 61, 1–13. https://doi.org/10.1109/TGRS.2023.3287334.
- Chung, H.M., Lavyton, D.C., 1995. Frequency characteristics of seismic reflections from thin beds. Can. J. Explor. Geophys. 31, 32–37.
- Dai, R.H., Yang, J., 2022. Seismic inversion with L2,0-norm joint-sparse constraint on multi-trace impedance model. Sci. Rep. 12 (1), 21811. https://doi.org/10.1038/ s41598-022-26488-1.
- Dasgupta, R., Clark, R.A., 1998. Estimation of Q from surface seismic reflection data. Geophysics 63 (6), 2120–2128. https://library.seg.org/doi/10.1190/1.1444505.
- Deng, H.B., Cheng, X.Y., Zeng, Y.J., et al., 2023. A high-resolution method of spectral fitting with horizon constraints and its application. J. Geophys. Eng. 20 (5), 901–914. https://doi.org/10.1093/jge/gxad042.
- Du, X., Li, G.F., Zhou, Z.X., et al., 2018. Band-controlled sparse deconvolution. Appl. Geophys. 155, 53–61. https://doi.org/10.1016/j.jappgeo.2018.05.012.
 Gao, Z.Q., Pan, Z.B., Gao, J.H., 2014. A new highly efficient differential evolution
- Gao, Z.Q., Pan, Z.B., Gao, J.H., 2014. A new highly efficient differential evolution scheme and its application to waveform inversion. Geosci. Rem. Sens. Lett. IEEE 11 (10), 1702–1706. https://doi.org/10.1109/LGRS.2014.2306263.
- Gholamy, A., Kreinovich, V., 2014. Why Ricker wavelets are successful in processing seismic data: towards a theoretical explanation. In: 2014 IEEE Symposium on Computational Intelligence for Engineering Solutions (CIES), Orlando, FL, USA, pp. 11–16. https://doi.org/10.1109/CIES.2014.7011824.
- Gibson, B., Larner, K., 1984. Predictive deconvolution and the zero-phase source. Geophysics 49 (4), 379–397. https://doi.org/10.1190/1.1441674.
- Grossman, J.P., Margrave, G.F., Lamoureux, M.P., et al., 2001. Constant-Q wavelet estimation via a nonstationary Gabor spectral model. In: CREWES Research Report, 13, pp. 223–240. https://www.crewes.org/Documents/ResearchReports/2001/2001-17.pdf.
- Guo, X., Gao, J.H., Yin, X.D., et al., 2022. Seismic high-resolution processing method based on spectral simulation and total variation regularization constraints. Appl. Geophys. 19 (1), 81–90. https://doi.org/10.1007/s11770-022-0927-5.
- Hu, Y., Chen, H., Lu, LQ, et al., 2020. An adaptive noise-free method of seismic resolution enhancement based on extrapolated multiresolution singular value decomposition. IEEE Trans. Geosci. Rem. Sens. 58 (7), 4958–4966. https://doi.org/10.1109/TGRS.2020.2970732.
- Jin, D.J., Eisner, E., 1984. A review of homomorphic deconvolution. Rev. Geophys. 22 (3), 255–263. https://doi.org/10.1029/RG022i003p00255.
- Lan, N.Y., Zhang, F.C., Sang, K.H., et al., 2023. Simultaneous denoising and resolution enhancement of seismic data based on elastic convolution dictionary learning. Pet. Sci. 20 (4), 2127–2140. https://doi.org/10.1016/j.petsci.2023.02.023.
- Lee, M.W., 1986. Spectral whitening in the frequency domain. US Geological Survey
- Li, Z.C., Li, D., Wang, D.Y., et al., 2013. Adaptive spectral modeling deconvolution based on the constraint of signal to noise ratio spectrum. Prog. Geophys. 28 (1), 301–309. https://doi.org/10.6038/pg20130133.
- Liu, N.H., Lei, Y.B., Liu, R.C., et al., 2023. Sparse time—frequency analysis of seismic data: sparse representation to unrolled optimization. IEEE Trans. Geosci. Rem. Sens. https://doi.org/10.1109/TGRS.2023.3300578.
- Ma, M., Wang, S.X., Yuan, S.Y., et al., 2017. Multichannel spatially correlated reflectivity inversion using block sparse Bayesian learning. Geophysics 82 (4), 191–199. https://doi.org/10.1190/geo2016-0366.1.
- Mamasani, M.G., Manaman, N.S., Kazemi, K., et al., 2017. Resolution enhancement of seismic data using spectral modeling based on dominant Ricker components and separable nonlinear least squares. Lead. Edge 36 (6), 480–486. https:// doi.org/10.1190/tle36060480.1.
- Margrave, G.F., 1998. Theory of nonstationary linear filtering in the Fourier domain with application to time-variant filtering. Geophysics 63 (1), 244–259. https://doi.org/10.1190/1.1444318.
- Margrave, G.F., Gibson, P.C., Grossman, J.P., et al., 2005. The Gabor transform, pseudodifferential operators, and seismic deconvolution. Integrated Comput. Aided Eng. 12 (1), 43–55. https://doi.org/10.3233/ICA-2005-12104.
- Margrave, G.F., Lamoureux, M., 2001. Gabor deconvolution. CREWES Res. Rep. 13, 241–276.
- Margrave, G.F., Lamoureux, M.P., Grossman, J.P., et al., 2002. Gabor deconvolution of seismic data for source waveform and Q correction. SEG Tech. Progr. Expand. Abstr. SEG 2002—2190. https://doi.org/10.1190/1.1817142.
- Mu, X.R., Mao, Q., Huang, J.P., 2023. Stable attenuation-compensated reverse time migration and its application to land seismic data. Pet. Sci. 20 (5), 2784–2795. https://doi.org/10.1016/j.petsci.2023.03.014.
- Naghadeh, D.H., Morley, C.K., 2017. Enhancement of temporal resolution using improved time-variant spectral whitening. J. Geophys. Eng. 14 (4), 822–832. https://doi.org/10.1088/1742-2140/aa6ddf.
- Ni, C.K., Su, M.J., Cheng, Y., et al., 2022. Thin-interbedded reservoirs prediction based on seismic sedimentology. Petrol. Explor. Dev. 49 (4), 851–863. https://doi.org/ 10.1016/51876-3804(22)60315-X.
- Ricker, N., 1953. The form and laws of propagation of seismic wavelets. Geophysics

- 18 (1), 10-40. https://doi.org/10.1190/1.1437843.
- Rosa, A.L.R., Ulrych, T.J., 1991. Processing via spectral modeling. Geophysics 56 (8), 1244–1251. https://doi.org/10.1190/1.1443144.
- Sajid, M., Ghosh, D., 2014. Logarithm of short-time Fourier transform for extending the seismic bandwidth. Geophys. Prospect. 62 (5), 1100–1110. https://doi.org/ 10.1111/1365-2478.12129.
- Sheriff, R.E., Geldart, L.P., 1995. Exploration Seismology. Explor. Seismol. Cambridge University Press.
- Stockwell, R.G., Mansinha, L., Lowe, R.P., 1996. Localization of the complex spectrum: the S transform. IEEE Trans. Signal Process. 44 (4), 998–1001. https://doi.org/10.1109/78.492555.
- Tang, B.W., Zhao, B., Wu, Y.H., et al., 2010. A new way to realize spectral modeling deconvolution. Oil Geophys. Prospect. 45, 66–70.
 Wang, D.Y., Huang, J.P., Kong, X., et al., 2017. Improving the resolution of seismic
- Wang, D.Y., Huang, J.P., Kong, X., et al., 2017. Improving the resolution of seismic traces based on the secondary time—frequency spectrum. Appl. Geophys. 14, 236–246. https://doi.org/10.1007/s11770-017-0616-v.
- Wang, Y.F., Zhou, H., Zhao, X.B., et al., 2019. CuQ-RTM: a CUDA-based code package for stable and efficient Q-compensated reverse time migration. Geophysics 84 (1), F1–F15. https://doi.org/10.1190/geo2017-0624.1.
- Widess, M.B., 1973. How thin is a thin bed? Geophysics 38 (6), 1176–1180. https://doi.org/10.1190/1.C0403.
- Wu, L., Castagna, J., 2017. S-transform and Fourier transform frequency spectra of broadband seismic signals. Geophysics 82 (5), 071–081. https://doi.org/ 10.1190/geo2016-0679.1.
- Wu, N.K., Zhou, H.L., Wang, Y.J., et al., 2020. Multichannel synchrosqueezing generalized S-transform for time-frequency analysis of seismic traces. Interpretation 8, 1–42. https://doi.org/10.1190/INT-2019-0172.1.
- Wu, J.Z., Shi, Y., Wang, W.H., et al., 2024. Improving image resolution using

- deabsorption prestack time migration with effective Q estimation: a back-propagation network approach. Geophysics 89 (1), S71–S82. https://doi.org/10.1190/geo2022-0753.1.
- Xu, S.G., Bao, Q.Z., Ren, Z.M., 2023. Target-oriented Q-compensated reverse-time migration by using optimized pure-mode wave equation in anisotropic media. Pet. Sci. 20 (2), 866–878. https://doi.org/10.1016/j.petsci.2022.12.016.
- Yang, Y., Wang, Z., Liu, N.H., et al., 2024. Physically driven self-supervised learning and its applications in geophysical inversion. IEEE Trans. Geosci. Rem. Sens. 62, 1–11. https://doi.org/10.1109/TGRS.2024.3368016.
- Zhang, C.J., Ulrych, T.J., 2002. Estimation of quality factors from CMP records. Geophysics 67 (5), 1542–1547. https://doi.org/10.1190/1.1512799.
- Zhang, R., Castagna, J., 2011. Seismic sparse-layer reflectivity inversion using basis pursuit decomposition. Geophysics 76 (6), R147—R158. https://doi.org/10.1190/ GEO2011-0103.1.
- Zhang, M.K., Gao, J.H., Wang, Z.G., et al., 2023. Enhancing seismic resolution via hyperbolic spaces S transform. IEEE Trans. Geosci. Rem. Sens. 61, 1–11. https:// doi.org/10.1109/TGRS.2023.3318253.
- Zhang, Y.Y., Wang, Y.Z., Shi, Y., et al., 2017. Frequencies of the ricker wavelet. Prog. Geophys. 32 (5), 2162–2167. https://doi.org/10.6038/pg2017054 (in Chinese). Zhang, Y.P., Zhou, H., Wang, Y.F., et al., 2022. A novel multichannel seismic decon-
- Zhang, Y.P., Zhou, H., Wang, Y.F., et al., 2022. A novel multichannel seismic deconvolution method via structure-oriented regularization. IEEE Trans. Geosci. Rem. Sens. 60, 1—10. https://doi.org/10.1109/TGRS.2022.3141113.
- Zhou, H.L., Tian, Y.M., Ye, Y., 2014. Dynamic deconvolution of seismic data based on generalized S-transform. J. Appl. Geophys. 108, 1–11. https://doi.org/10.1016/j.jappgeo.2014.06.004.
- Zhou, W., Zhou, H.L., Long, D., et al., 2024. Time frequency domain combined deconvolution method. Acta Geophys. 72 (2), 727–741. https://doi.org/10.1007/s11600-023-01129-x.